GEOLOGY | THE GEOLOGICAL SOCIETY OF AMERICA®

https://doi.org/10.1130/G49028.1

Manuscript received 13 November 2020
Revised manuscript received 3 March 2021
Manuscript accepted 28 April 2021

A new kind of invisible gold in pyrite hosted in deformation-related dislocations

Denis Fougerouse[1,2], Steven M. Reddy[1,2], Mark Aylmore[2], Lin Yang[3], Paul Guagliardo[4], David W. Saxey[2], William D.A. Rickard[2] and Nicholas Timms[1]

[1]School of Earth and Planetary Sciences, Curtin University, Perth, WA 6845, Australia
[2]Geoscience Atom Probe Facility, John de Laeter Centre, Curtin University, Perth, WA 6102, Australia
[3]State Key Laboratory of Geological Processes and Mineral Resources, China University of Geosciences, Beijing 100083, China
[4]Centre for Microscopy, Characterisation and Analysis, The University of Western Australia, Crawley, WA 6009, Australia

ABSTRACT

Mining of "invisible gold" associated with sulfides in gold ores represents a significant proportion of gold production worldwide. Gold hosted in sulfide minerals has been proposed to be structurally bound in the crystal lattice as a sulfide-gold alloy and/or to occur as discrete metallic nanoparticles. Using a combination of microstructural quantification and nanoscale geochemical analyses on a pyrite crystal from an orogenic gold deposit, we show that dislocations hosted in a deformation low-angle boundary can be enriched in Ni, Cu, As, Pb, Sb, Bi, and Au. The cumulative trace-element enrichment in the dislocations is 3.2 at% higher compared to the bulk crystal. We propose that trace elements were segregated during the migration of the dislocation following the dislocation-impurity pair model. The gold hosted in nanoscale dislocations represents a new style of invisible gold.

INTRODUCTION

The discovery rate of new gold deposits is in decline worldwide, with the ore quality degrading in parallel to the precious metal value increasing. Ores with invisible gold are characterized by trace amounts of gold hosted in sulfide minerals (from a few parts per million to several thousand parts per million), predominantly pyrite and arsenopyrite (Cook and Chryssoulis, 1990), and this is now a common resource for the gold mining industry. In these ores, gold is either structurally bound in the crystal lattice as an alloy (Cabri et al., 1989), or it occurs as discrete metallic nanoparticles and microparticles (Palenik et al., 2004).

Recently, it has been postulated that gold can be hosted in low-angle boundaries (Dubosq et al., 2018; Wu et al., 2021). However, along deformation microstructures, the nature of the gold (native gold or alloyed), its mineralogical location (solid solution, crystal defects, or open fractures), its source (intragrain/intergrain diffusion or secondary fluid-related), and the mechanisms for gold segregation are unresolved. Determining the form and distribution of gold in refractory ores has been technically challenging because the analytical volume of many quantitative approaches is far greater than the size of the gold particles in sulfides (Fougerouse et al., 2020). Therefore, relationships between gold and deformation microstructures have remained speculative.

Characterization of the processes responsible for its chemical modification underpins the widespread use of pyrite to both constrain the formation of ore deposits and to optimize extraction of the gold it contains (Cook et al., 2013). The bulk chemical compositions of sulfide mineral assemblages have therefore been well documented, but the processes by which the chemistry of pyrite may have been modified are still debated.

In order to better understand the crystallographic location of gold in deformation microstructures, we used nanoscale characterization techniques on gold-bearing arsenian pyrite that underwent a low amount of crystal plasticity. The results advance our understanding of the process by which pyrite chemistry can be modified and also suggest an alternative interpretation to anomalous geochemical spot analyses, commonly attributed to nanoparticles. The implications of the results for the selective extraction of gold are also conceptualized.

SAMPLES AND METHODS

The studied sample was collected in the Huangjindong orogenic-type gold deposit, hosted in the central part of the Jiangnan orogen (Fig. 1; Zhang et al., 2020). The Jiangnan orogen was formed during the collision between the Yangtze and Cathaysia blocks during the assembly of the Rodinia supercontinent (Li et al., 2008). The sample (D02B3; 114.049°N, 28.675°E; Fig. 1) is a representative gold ore from east-west–trending orebodies (dipping 45–70°S; Zhang et al., 2020). The sample is a mineralized slate with a stock work of small (a few centimeters) quartz veins (Fig. 1). The main ore minerals include pyrite and arsenopyrite with minor chalcopyrite, tetrahedrite, galena, and native gold (Zhang et al., 2020). At Huangjindong, gold mainly occurs within arsenopyrite or pyrite with gold concentrations of several hundreds of parts per million in pyrite (Zhang et al., 2020). The gold-rich pyrites are synmineralization minerals and formed at temperature of 200–350 °C (see the Supplemental Material[1]; Li et al., 2011) above the brittle-ductile transition temperature of 200 °C defined for pyrite (Barrie et al., 2009).

A pyrite grain from a slate-hosted aggregate was analyzed by electron backscattered diffraction (EBSD) using a TESCAN Clara scanning electron microscope (SEM) equipped with an Oxford Instruments Symmetry EBSD detector. We selected an ~2° low-angle boundary

[1]Supplemental Material. Supplemental geological context, analytical methods, and supporting data. Please visit https://doi.org/10.1130/GEOL.S.14772060 to access the supplemental material, and contact editing@geosociety.org with any questions.

CITATION: Fougerouse, D., et al., 2021, A new kind of invisible gold in pyrite hosted in deformation-related dislocations: Geology, v. 49, p. , https://doi.org/10.1130/G49028.1

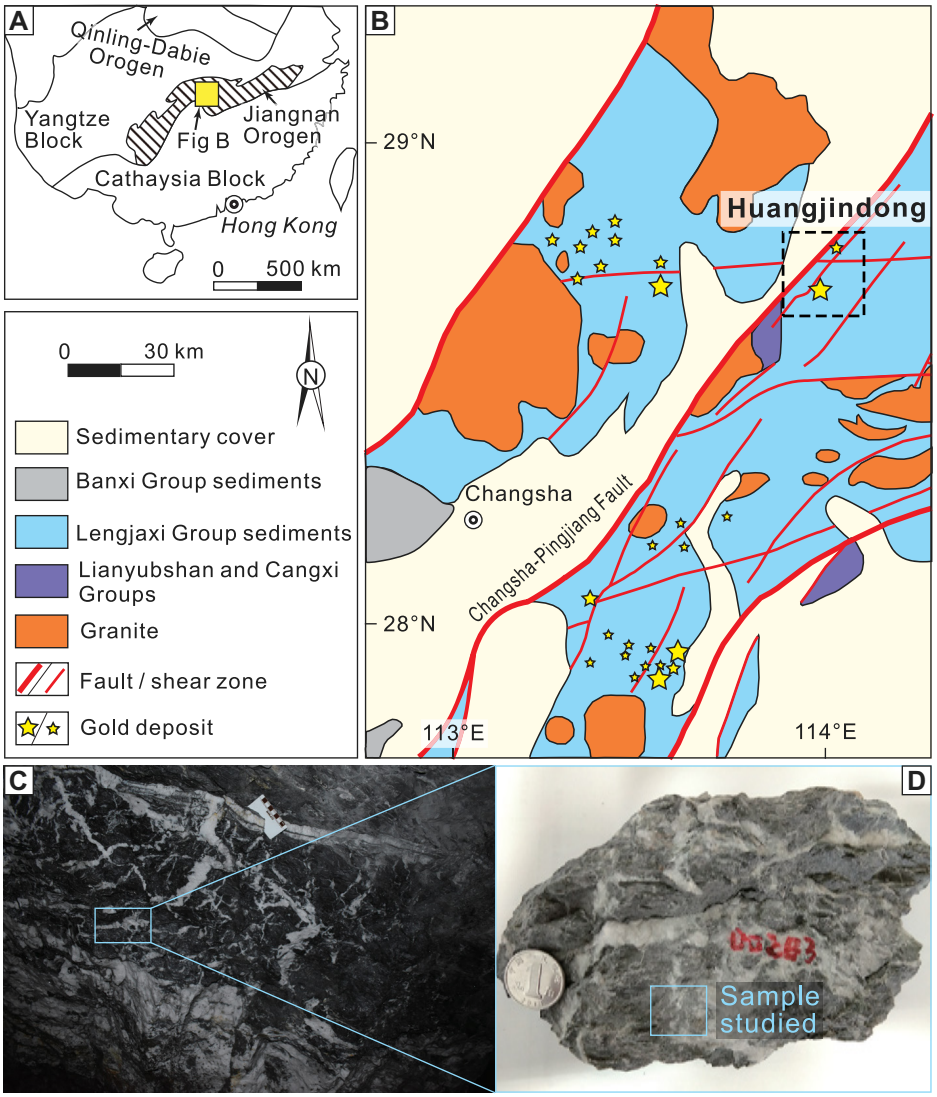

Figure 1. (A) Simplified geological map of southern China. (B) Simplified geological map of the Changsha-Pingjiang fault zone showing distribution of main rock units and faults/shear zones, and locations of Huangjindong and other gold deposits (modified from Zhang et al., 2020). (C) Field photograph showing location of gold ore sample D02B3. (D) Hand sample photograph and location of polished block.

within the pyrite for nanoscale secondary ion mass spectrometry (NanoSIMS) analyses using a CAMECA NanoSIMS 50L. A TESCAN Lyra3 Ga^+ focused ion beam SEM (FIB-SEM) was used to prepare atom probe needle-shaped specimens following the Pt button targeting approach (Rickard et al., 2020). Atom probe tomography (APT) specimens were analyzed with the CAMECA LEAP 4000X HR Geoscience Atom Probe in the John de Laeter Centre at Curtin University (Perth, Australia). Details of the approach for geological materials are given elsewhere (Reddy et al., 2020). Additional technical information is provided in the Supplemental Material.

RESULTS

The pyrite is a single large grain (400 × 800 μm; Fig. 2) with a few micrometer-sized inclusions of arsenopyrite. The EBSD data revealed lattice distortion within the grain with a maximum distortion of ~10°. Internally, this distortion is manifest by subtle lattice orientation variations (<1°) and the presence of a few discrete low-angle boundaries with ~2° disorientation (Fig. 2). The EBSD data indicate that many of the boundaries are consistent with operation of the {100}<010> slip system, which is common in pyrite (Fig. 2). However, one boundary has misorientation axes close to <110>, indicating the likely dominance of $\{1\bar{1}0\}<010>$ slip, associated with a <110> dislocation line (Fig. 2E). This slip system has been previously identified from EBSD analyses of deformed pyrite (Barrie et al., 2008). This boundary showed no evidence of microfractures, indicating the coherent nature of the microstructure.

NanoSIMS data showed that the As distribution at the microscale is heterogeneous with two domains marked by oscillatory zoning at a high angle to one another (Fig. 2D). One of these domains is enriched in gold, whereas the second domain is gold-poor. The gold-rich domain represents the majority of the gold budget in this weakly deformed crystal. Isolated areas enriched in gold are spatially linked with crosscutting microfractures and/or As-rich domains, including the boundary targeted by EBSD data. This boundary is enriched in gold and cuts across all domains (Fig. 2C). APT targeted the low-angle boundary in the gold-rich region of the pyrite.

The nanoscale characterization of the low-angle boundary by APT revealed that the boundary plane is oriented oblique to the specimen axis and composed of parallel, trace-element–rich linear features spaced 10–15 nm (Fig. 3; Fig. S2). The linear features are subhorizontal within the plane of the boundary and are decorated with Ni, Cu, As, Pb, Sb, Bi, and Au (Table 1). The total trace-element concentration in the dislocations reaches ~4.5 at% (atomic percent), compared to 1.3 at% in the bulk of the APT specimen. The trace-element enrichment is compensated by a decrease in Fe (~2.8 at% decrease) and S (~0.4 at% decrease). The gold concentration in the dislocations is 253 ± 26 ppma (1σ), but it is below the detection limit outside of the low-angle boundary. When viewed in three dimensions, the gold atoms do not form large or dense clusters, and gold is unlikely to form discrete nanoparticles (Fougerouse et al., 2016). Concentration profiles generated normal to the boundary and through single dislocations revealed that the As concentration is enriched in the dislocation (from ~1.3 to ~2 at%) and depleted in its close vicinity (from ~1.3 to ~1 at%; Fig. 3) compared to the bulk composition. The depleted zones extend 10–15 nm and are confined to either one side of the boundary or the other, exclusively (Fig. 3). Outside the dislocation, other trace elements are below detection limits in the concentration profiles.

TRACE ELEMENT–ENRICHED CRYSTAL DEFECTS

The Au and As oscillatory texture observed on the NanoSIMS images is common in sulfides, and gold is typically hosted in solid solution or as nanoparticles within these domains (Reich et al., 2005; Fougerouse et al., 2016; Gopon et al., 2019; Wu et al., 2019). The dominant mechanism to produced oscillatory zoning is generally accepted to be the diffusion-limited self-organization of ions at the crystal-fluid interface, which can produce nanoscale domains during crystal growth (Putnis et al., 1992; Wu et al., 2019). The origin of spurious gold along microfractures is unclear and may be real or an analysis artifact due to topographical effects (Fig. 2).

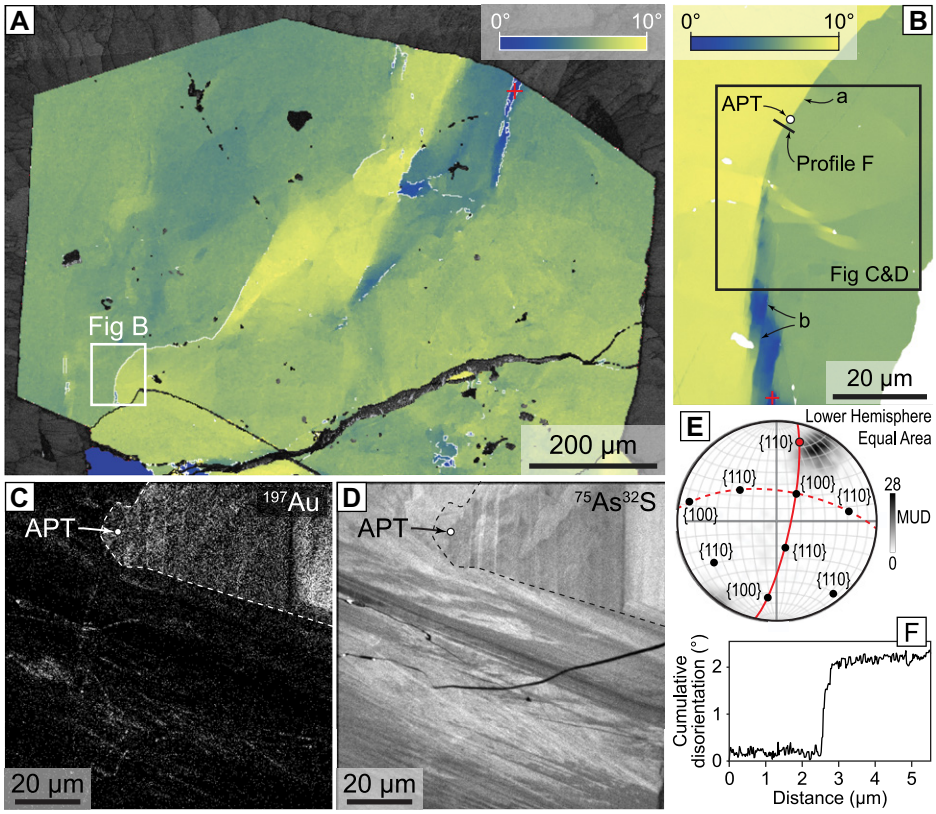

Figure 2. Grain-scale crystallography and chemistry. (A,B) Crystallographic orientation electron backscattered diffraction (EBSD) map. Misorientation is color-coded from reference point "+" to a maximum of 10°. Low-angle boundaries (>1°) are plotted in white in A. Location of atom probe tomography (APT) specimens 1 and 2 are labeled. (C,D) Nanoscale secondary ion mass spectrometry (NanoSIMS) maps of ^{197}Au and ^{75}As^{32}S revealing heterogeneous distribution of Au and As. Boundary "a" is highlighted by linear enrichment of gold. Dashed line represents boundary between gold-rich and gold-poor domains. (E) Lower-hemisphere, equal-area projection of pyrite lattice orientations at the site of atom probe specimens. Red dot represents dominant misorientation axis in the region of interest and most likely orientation of dislocations. Two red great circles represent {100} planes away from the region of interest at location "b." MUD—multiple of uniform density. (F) Cumulative disorientation profile highlighting 2° low-angle boundary.

Comparison between the geometry of the nanoscale linear features observed in the plane of the low-angle boundary and the EBSD data from this particular boundary shows that these linear features are most consistent with <110> dislocations (Fig. 2). The linear features are also consistent with dislocations imaged by APT in other minerals (Piazolo et al., 2016; Kirkland et al., 2018; Fougerouse et al., 2019; Schipper et al., 2020). Trace-element enrichment in the dislocation is up to 3.2 at% increase, including Ni, Cu, As, Pb, Sb, Bi, and Au (Table 1). It is unclear whether the trace elements hosted in the dislocation are substituted on Fe sites, or if they have precipitated as a separate phase along the dislocation similar to Fe-As-Sb-Pb-Ni-Au-S nanoparticles observed in pyrite (Deditius et al., 2011).

The absence of microfracturing along the low-angle boundary and the coherent nature of the boundary as observed by the dislocation's orientation using APT and correlative techniques favor a diffusion-driven trace-element redistribution model rather than a fluid-mediated process. Three diffusion models are commonly proposed, including solid-state (volume) diffusion, short-circuit pathways diffusion, and defect-impurity pair diffusion (Mehrer, 2007). The solid-state diffusion of an element is only considered efficient at high temperatures and is unlikely to have been significant at the temperature experienced at the Huangjindong deposit (200–350 °C; Mehrer, 2007; Li et al., 2011).

Our data reveal that the As concentration is depleted by ~0.3 at% in a 10–15-nm-wide zone on one side or the other of the dislocations (Fig. 3). During crystal-plastic deformation, low-angle boundaries form by the rearrangement of dislocations into a plane with dislocations migrating from both sides of the boundary (Hull and Bacon, 2001). Migrating dislocations have the capability to capture impurities (Cottrell and Bilby, 1949). The As depletion zone in close proximity to the dislocation may represent the capture zone of the dislocation (Dubosq et al., 2019), with dislocations originating from both sides of the boundary. This capture zone may only be transient in the eventuality that As is reincorporated into the crystal structure during dislocation migration, as recently proposed for Ca during twining in monazite (Fougerouse et al., 2021). The As distribution is therefore consistent with the defect-impurity pair model (Mehrer, 2007). Gold and other trace elements were not detected above the detection limit in the concentration profiles, and their behavior during deformation cannot be directly evaluated. However, it is well recognized that As and Au have a coupled behavior in pyrite (Reich et al., 2005), and it is reasonable to assume that gold was captured by the dislocations during their migration following the defect-impurity pair diffusion model responsible for As mobility.

Alternatively, the NanoSIMS data reveal that the low-angle boundary is crosscut by microfractures, which could have been the source of gold diffusing along the low-angle boundary following the high-diffusivity pathway model. However, the presence of an efficient chemical gradient that would drive diffusion in the pyrite studied is questionable due to only minor compositional differences between the gold-rich and gold-poor domains (Manning and Bruner, 1968). Still, the high-diffusivity pathway model cannot be discounted to account for gold along dislocations.

Regardless of the mechanism responsible for gold enrichment in dislocations, such crystallographic locations represent a new type of gold habit in pyrite related to defects that was previously "invisible" to other analytical techniques.

IMPLICATIONS OF DISLOCATION-HOSTED GOLD IN SULFIDE ORES

In pyrite geochemical studies, infrequent anomalously high counts in time-resolved output graphs from laser ablation–inductively coupled plasma–mass spectrometry (LA-ICP-MS) are commonly attributed to the presence of discrete mineral inclusions (Gregory et al., 2015). Our study, however, shows that anomalous element concentrations can also be directly related to deformation microstructures.

The nature of the gold-bearing phase along the dislocation, i.e., pyrite with a high trace-element composition or a separate phase, remains unresolved from our results. Although the former scenario is the classic view of decorated dislocations in deformed minerals, the latter would represent a previously unrecognized phenomenon in the earth sciences. Such structures, labeled linear complexions, have been described in the materials science literature (Kuzmina et al., 2015) but have not been recognized in naturally deformed minerals. The effect of linear complexions on mineral grain boundary stability is untested in the literature and is not taken into consideration in quantitative deformation models (Ran et al., 2019). The chemistry

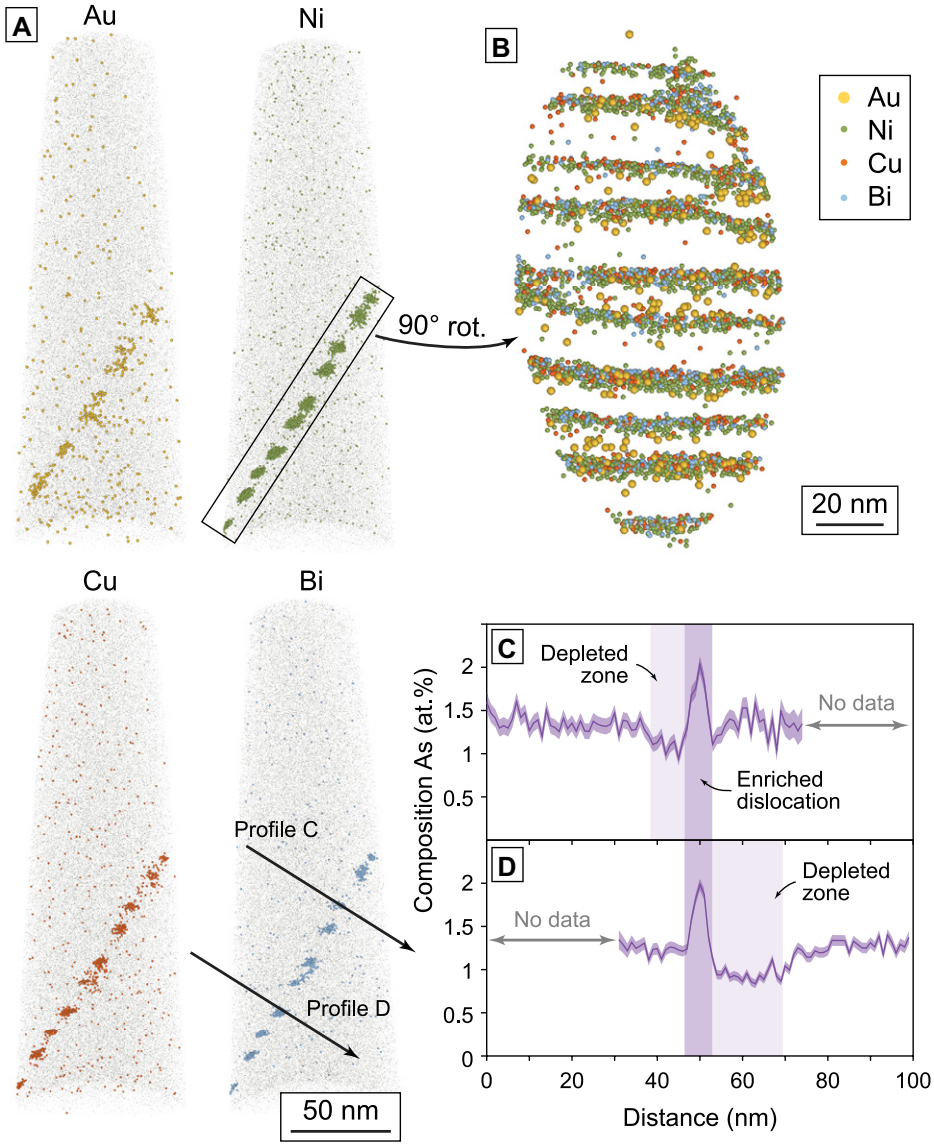

Figure 3. Nanoscale imaging of low-angle boundary (specimen 1). (A,B) Each sphere represents an atom. Low-angle boundary plane is composed of subhorizontal Au-, Ni-, Cu-, and Bi-enriched dislocations. (C,D) One-dimensional (1-D) concentration profiles for As showing depletion on one side of dislocation or the other, exclusively.

of deformation microstructures and the pyrite composition prior to deformation may therefore have an influence on its crystal-plastic behavior under stress; however, these parameters are generally not tested in deformation experiments (Barrie et al., 2009). The gap in knowledge surrounding linear complexions in minerals therefore warrants further investigation, including the confirmation by correlative techniques to test whether a different phase can be present along dislocations in minerals.

TABLE 1. MAJOR- (AT%) AND TRACE-ELEMENT (PPMA) COMPOSITIONS OF DISLOCATIONS BY ATOM PROBE TOMOGRAPHY

Element	Dislocation	Uncertainty (1σ)
Fe	36.67	0.11
S	58.80	0.16
As	3.19	0.03
Au	253	26
Ni	7141	136
Cu	1217	56
Sb	803	46
Pb	2213	76
Bi	1466	62

Most refractory gold ores require oxidation of the sulfides to liberate gold locked as "solid solution" or as very fine inclusions. Studies of strained crystals in other mineral systems indicate enhanced nonlinear dissolution in the presence of crystal defects such as dislocations (Lasaga and Luttge, 2001). Despite the common occurrence of pyrite crystal-plastic deformation textures, even at low temperature (Barrie et al., 2009), no studies have focused on the effects of crystal-plastic deformation microstructures on dissolution processes in sulfide minerals. The predictions from other strained minerals suggest that pyrite dislocations enriched in gold could be more prone to dissolution than bulk crystal, thus reducing energy consumption necessary for extraction. This enhanced dissolution of gold-enriched domains should be investigated as an alternative method of selective or in situ leaching (Heath et al., 2008).

In the Huangjindong gold deposit, the majority of the pyrite-hosted gold is contained in the oscillatory zones in the pyrite. However, the budget of gold hosted in deformation microstructures may be dominant over structurally bound gold in highly deformed pyrites. Accurate quantification of the deformation microstructures in invisible gold ores could lead to processing options tailored to highly deformed gold deposits in polymetamorphic terranes commonly hosting orogenic-type gold deposits.

ACKNOWLEDGMENTS

The study was supported by the Australian Science and Industry Endowment Fund (grant SIEF RI13–01). Fougerouse acknowledges Australian Research Council funding DE190101307. Lin Yang thanks Liqiang Yang, Qingfei Wang, and Liang Zhang for assistance with sample collection. We are grateful for constructive reviews by Renelle Dubosq, Anna Rogowitz, and an anonymous reviewer, and editorial handling by Dennis Brown and Jerry Dickens.

REFERENCES CITED

Barrie, C.D., Boyle, A.P., Cox, S.F., and Prior, D.J., 2008, Slip systems and critical resolved shear stress in pyrite: An electron backscatter diffraction (EBSD) investigation: Mineralogical Magazine, v. 72, p. 1181–1199, https://doi.org/10.1180/minmag.2008.072.6.1181.

Barrie, C.D., Boyle, A., and Salter, M., 2009, How low can you go?—Extending downwards the limits of plastic deformation in pyrite: Mineralogical Magazine, v. 73, p. 895–913, https://doi.org/10.1180/minmag.2009.073.6.895.

Cabri, L.J., Chryssoulis, S.L., de Villiers, J.P., Laflamme, J.G., and Buseck, P.R., 1989, The nature of "invisible" gold in arsenopyrite: Canadian Mineralogist, v. 27, p. 353–362.

Cook, N.J., and Chryssoulis, S.L., 1990, Concentrations of invisible gold in the common sulfides: Canadian Mineralogist, v. 28, p. 1–16.

Cook, N.J., Ciobanu, C.L., Meria, D., Silcock, D., and Wade, B., 2013, Arsenopyrite-pyrite association in an orogenic gold ore: Tracing mineralization history from textures and trace elements: Economic Geology and the Bulletin of the Society of Economic Geologists, v. 108, p. 1273–1283, https://doi.org/10.2113/econgeo.108.6.1273.

Cottrell, A.H., and Bilby, B., 1949, Dislocation theory of yielding and strain ageing of iron: Proceedings of the Physical Society, A, v. 62, p. 49, https://doi.org/10.1088/0370-1298/62/1/308.

Deditius, A.P., Utsunomiya, S., Reich, M., Kesler, S.E., Ewing, R.C., Hough, R., and Walshe, J., 2011, Trace metal nanoparticles in pyrite: Ore Geology Reviews, v. 42, p. 32–46, https://doi.org/10.1016/j.oregeorev.2011.03.003.

Dubosq, R., Lawley, C., Rogowitz, A., Schneider, D., and Jackson, S., 2018, Pyrite deformation and connections to gold mobility: Insight from micro-structural analysis and trace element mapping: Lithos, v. 310, p. 86–104, https://doi.org/10.1016/j.lithos.2018.03.024.

Dubosq, R., Rogowitz, A., Schweinar, K., Gault, B., and Schneider, D.A., 2019, A 2D and 3D nanostructural study of naturally deformed

pyrite: Assessing the links between trace element mobility and defect structures: Contributions to Mineralogy and Petrology, v. 174, p. 72, https://doi.org/10.1007/s00410-019-1611-5.

Fougerouse, D., Reddy, S.M., Saxey, D.W., Rickard, W.D., Van Riessen, A., and Micklethwaite, S., 2016, Nanoscale gold clusters in arsenopyrite controlled by growth rate not concentration: Evidence from atom probe microscopy: The American Mineralogist, v. 101, p. 1916–1919, https://doi.org/10.2138/am-2016-5781CCBYNCND.

Fougerouse, D., Reddy, S.M., Kirkland, C.L., Saxey, D.W., Rickard, W.D., and Hough, R.M., 2019, Time-resolved, defect-hosted, trace element mobility in deformed Witwatersrand pyrite: Geoscience Frontiers, v. 10, p. 55–63, https://doi.org/10.1016/j.gsf.2018.03.010.

Fougerouse, D., Kirkland, C.L., Saxey, D.W., Seydoux-Guillaume, A.M., Rowles, M.R., Rickard, W.D.A., and Reddy, S.M., 2020, Nanoscale isotopic dating of monazite: Geostandards and Geoanalytical Research, v. 44, p. 637–642, https://doi.org/10.1111/ggr.12340.

Fougerouse, D., Reddy, S., Seydoux-Guillaume, A.-M., Kirkland, C., Erickson, T., Saxey, D., Rickard, W., Jacob, D., Leroux, H., and Clark, C., 2021, Mechanical twinning of monazite expels radiogenic lead: Geology, v. 49, p. 417–421, https://doi.org/10.1130/G48400.1.

Gopon, P., Douglas, J.O., Auger, M.A., Hansen, L., Wade, J., Cline, J.S., Robb, L.J., and Moody, M.P., 2019, A nanoscale investigation of Carlin-type gold deposits: An atom-scale elemental and isotopic perspective: Economic Geology and the Bulletin of the Society of Economic Geologists, v. 114, p. 1123–1133, https://doi.org/10.5382/econgeo.4676.

Gregory, D.D., Large, R.R., Halpin, J.A., Baturina, E.L., Lyons, T.W., Wu, S., Danyushevsky, L., Sack, P.J., Chappaz, A., and Maslennikov, V.V., 2015, Trace element content of sedimentary pyrite in black shales: Economic Geology and the Bulletin of the Society of Economic Geologists, v. 110, p. 1389–1410, https://doi.org/10.2113/econgeo.110.6.1389.

Heath, J., Jeffrey, M., Zhang, H., and Rumball, J., 2008, Anaerobic thiosulfate leaching: Development of in situ gold leaching systems: Minerals Engineering, v. 21, p. 424–433, https://doi.org/10.1016/j.mineng.2007.12.006.

Hull, D., and Bacon, D.J., 2001, Introduction to Dislocations: Oxford, UK, Butterworth-Heinemann, 272 p.

Kirkland, C.L., Fougerouse, D., Reddy, S.M., Hollis, J., and Saxey, D.W., 2018, Assessing the mechanisms of common Pb incorporation into titanite: Chemical Geology, v. 483, p. 558–566, https://doi.org/10.1016/j.chemgeo.2018.03.026.

Kuzmina, M., Herbig, M., Ponge, D., Sandlöbes, S., and Raabe, D., 2015, Linear complexions: Confined chemical and structural states at dislocations: Science, v. 349, p. 1080–1083, https://doi.org/10.1126/science.aab2633.

Lasaga, A.C., and Luttge, A., 2001, Variation of crystal dissolution rate based on a dissolution stepwave model: Science, v. 291, p. 2400–2404, https://doi.org/10.1126/science.1058173.

Li, J., Chen, B., An, J., Tan, S., Zhang, X., and Yao, Y., 2011, Characteristics of fluid inclusions of the Huangjindong gold deposit, Hunan Province: Geology and Mineral Resources of South China, v. 27, p. 163–168.

Li, Z.-X., Bogdanova, S., Collins, A., Davidson, A., De Waele, B., Ernst, R., Fitzsimons, I., Fuck, R., Gladkochub, D., and Jacobs, J., 2008, Assembly, configuration, and break-up history of Rodinia: A synthesis: Precambrian Research, v. 160, p. 179–210, https://doi.org/10.1016/j.precamres.2007.04.021.

Manning, J.R., and Bruner, L., 1968, Diffusion kinetics for atoms in crystals: American Journal of Physics, v. 36, p. 922–923, https://doi.org/10.1119/1.1974325.

Mehrer, H., 2007, Diffusion in Solids: Fundamentals, Methods, Materials, Diffusion-Controlled Processes: Berlin, Springer Science & Business Media, Springer Series in Solid-State Sciences 155, 654 p., https://doi.org/10.1007/978-3-540-71488-0.

Palenik, C.S., Utsunomiya, S., Reich, M., Kesler, S.E., Wang, L., and Ewing, R.C., 2004, "Invisible" gold revealed: Direct imaging of gold nanoparticles in a Carlin-type deposit: The American Mineralogist, v. 89, p. 1359–1366, https://doi.org/10.2138/am-2004-1002.

Piazolo, S., La Fontaine, A., Trimby, P., Harley, S., Yang, L., Armstrong, R., and Cairney, J.M., 2016, Deformation-induced trace element redistribution in zircon revealed using atom probe tomography: Nature Communications, v. 7, 10490, https://doi.org/10.1038/ncomms10490.

Putnis, A., Fernandez-Diaz, L., and Prieto, M., 1992, Experimentally produced oscillatory zoning in the $(Ba, Sr)SO_4$ solid solution: Nature, v. 358, p. 743–745, https://doi.org/10.1038/358743a0.

Ran, H., de Riese, T., Llorens, M.-G., Finch, M.A., Evans, L.A., Gomez-Rivas, E., Griera, A., Jessell, M.W., Lebensohn, R.A., and Piazolo, S., 2019, Time for anisotropy: The significance of mechanical anisotropy for the development of deformation structures: Journal of Structural Geology, v. 125, p. 41–47, https://doi.org/10.1016/j.jsg.2018.04.019.

Reddy, S.M., Saxey, D.W., Rickard, W.D.A., Fougerouse, D., Montalvo, S.D., Verberne, R., and van Riessen, A., 2020, Atom probe tomography: Development and application to the geosciences: Geostandards and Geoanalytical Research, v. 44, p. 5–50, https://doi.org/10.1111/ggr.12313.

Reich, M., Kesler, S.E., Utsunomiya, S., Palenik, C.S., Chryssoulis, S.L., and Ewing, R.C., 2005, Solubility of gold in arsenian pyrite: Geochimica et Cosmochimica Acta, v. 69, p. 2781–2796, https://doi.org/10.1016/j.gca.2005.01.011.

Rickard, W.D., Reddy, S.M., Saxey, D.W., Fougerouse, D., Timms, N.E., Daly, L., Peterman, E., Cavosie, A.J., and Jourdan, F., 2020, Novel applications of FIB-SEM-based ToF-SIMS in atom probe tomography workflows: Microscopy and Microanalysis, v. 26, p. 750–757, https://doi.org/10.1017/S1431927620000136.

Schipper, C.I., Rickard, W.D.A., Reddy, S.M., Saxey, D.W., Castro, J.M., Fougerouse, D., Quadir, Z., Conway, C., Prior, D.J., and Lilly, K., 2020, Volcanic SiO_2-cristobalite: A natural product of chemical vapor deposition: The American Mineralogist, v. 105, p. 510–524, https://doi.org/10.2138/am-2020-7236.

Wu, Y.-F., Fougerouse, D., Evans, K., Reddy, S.M., Saxey, D.W., Guagliardo, P., and Li, J.-W., 2019, Gold, arsenic, and copper zoning in pyrite: A record of fluid chemistry and growth kinetics: Geology, v. 47, p. 641–644, https://doi.org/10.1130/G46114.1.

Wu, Y.-F., Evans, K., Hu, S.-Y., Fougerouse, D., Zhou, M.-F., Fisher, L.A., Guagliardo, P., and Li, J.-W., 2021, Decoupling of Au and As during rapid pyrite crystallization: Geology, v. 49, p. 827–831, https://doi.org/10.1130/G48443.1 (in press).

Zhang, L., Groves, D.I., Yang, L.-Q., Sun, S.-C., Weinberg, R.F., Wang, J.-Y., Wu, S.-G., Gao, L., Yuan, L.-L., and Li, R.-H., 2020, Utilization of pre-existing competent and barren quartz veins as hosts to later orogenic gold ores at Huangjindong gold deposit, Jiangnan orogen, southern China: Mineralium Deposita, v. 55, p. 363–380, https://doi.org/10.1007/s00126-019-00904-5.

Printed in USA